remote sensing

MDPI

Article

Assessing Shallow Soft Deposits through Near-Surface Geophysics and UAV-SfM: Application in Pocket Beaches Environments

Luciano Galone [1], Sebastiano D'Amico [1,*], Emanuele Colica [1,2], Peter Iregbeyen [1], Pauline Galea [1], Lluís Rivero [3] and Fabio Villani [4]

[1] Department of Geosciences, University of Malta, MSD2080 Msida, Malta; luciano.galone@um.edu.mt (L.G.); emanuele.colica@um.edu.mt (E.C.); peter.iregbeyen@um.edu.mt (P.I.); pauline.galea@um.edu.mt (P.G.)
[2] Research & Planning Unit, Public Works Department, Ministry for Public Works and Planning, Project House, Triq Francesco Buonamici, FRN1700 Floriana, Malta
[3] Department of Mineralogy, Petrology and Applied Geology, Earth Sciences Faculty, University of Barcelona, 08028 Barcelona, Spain; lrivero@ub.edu
[4] Istituto Nazionale di Geofisica e Vulcanologia, 00143 Rome, Italy; fabio.villani@ingv.it
* Correspondence: sebastiano.damico@um.edu.mt

Abstract: This study employs a multimethod approach to investigate the sediment distribution in two pocket beaches, Ramla Beach and Mellieha S Beach, in Malta. Both study sites were digitally reconstructed using unmanned aerial vehicle (UAV) photogrammetry. For each case, an ERT and a dense network of ambient seismic noise measurements processed through a horizontal-to-vertical spectral ratio (HVSR) technique were acquired. Electrical resistivity tomography (ERT) analysis enables the estimation of sediment thickness in each beach. HVSR analysis revealed peaks related to beach sediments overlying limestone rocks in both sites and also indicated a deeper stratigraphic contact in Mellieha S Beach. Based on ERT measurements, sediment thickness is calculated for each HVSR measurement. Interpolation of results allows for bedrock surface modelling in each case study, and when combined with digital terrain models (DTMs) derived from photogrammetric models, sediment volumes are estimated for each site. The geometry of this surface is analyzed from a geological perspective, showing structural control of sediment distribution due to a normal fault in Mellieha S Beach and stratigraphic control facilitated by a highly erodible surface in Ramla Beach. The results emphasize the importance of adopting a three-dimensional perspective in coastal studies for precise sediment volume characterization and a deeper understanding of pocket beach dynamics. This practical multimethod approach presented here offers valuable tools for future coastal research and effective coastal management, facilitating informed decision making amidst the growing vulnerability of coastal zones to climate change impacts.

Keywords: horizontal-to-vertical spectral ratio; seismic ambient noise; pocket beach; Malta; near-surface geophysics; electrical resistivity tomography; photogrammetry

Citation: Galone, L.; D'Amico, S.; Colica, E.; Iregbeyen, P.; Galea, P.; Rivero, L.; Villani, F. Assessing Shallow Soft Deposits through Near-Surface Geophysics and UAV-SfM: Application in Pocket Beaches Environments. *Remote Sens.* **2024**, *16*, 40. https://doi.org/10.3390/rs16010040

Academic Editor: José Juan de Sanjosé Blasco

Received: 30 October 2023
Revised: 14 December 2023
Accepted: 18 December 2023
Published: 21 December 2023

1. Introduction

Estimating the thickness of shallow, non-consolidated sedimentary deposits is a common challenge in geology, engineering, and environmental sciences in general. Particularly, understanding sediment thickness in beaches is crucial for scientific research, modelling of erosional and depositional processes, and informed decision making for coastal protection infrastructure. Accurate estimation of sediment volumes in coastal areas is important for a comprehensive understanding of littoral processes, sediment budget studies and geomorphological evolution [1]. However, in these studies, the lower boundary of beach sedimentary deposits is rarely estimated (e.g., [2]) due to the difficulty of data acquisition.

While coring or trenching offers direct measurements of sediment thickness, these methods can be costly, labor-intensive, limited in spatial coverage, and may even, in some cases, be restricted due to ecological or normative reasons that hamper their acquisition.

To address these limitations, geophysical approaches have emerged as promising methods [3]. Nevertheless, the non-uniqueness of results in the inversion process, inherent to the geophysical method, is a limitation to determining the exact sediment thickness solely based on one technique. To ensure the reliability of the results, calibration and validation of sediment thickness estimates by using independent approaches, such as geological data or other geophysical techniques, are necessary.

In this study, we aim to reconstruct the 3D sediment distribution in a dynamic environment by combining surface and subsurface information, utilizing horizontal-to-vertical spectral ratio (HVSR) of ambient seismic noise, supported by electrical resistivity tomography (ERT) and structure from motion (SfM) photogrammetry from unmanned aerial systems (UAV).

The HVSR [4] method is a passive seismic technique that utilizes a three-component seismometer to measure the vertical and horizontal components of ambient seismic noise. The noise from approximately 0.1 to 1 Hz is generated by sources such as ocean waves, extensive regional storms and tectonic activity, while frequencies above 1 Hz typically originate from closer sources, including local storms, wind and human-made activities [5]. HVSR has been widely applied in sediment thickness estimation-related studies in different environments due to its simplicity in field acquisition and processing [6–9], including some applications on beaches [3,10,11]. Its complementarity with ERT, which utilizes active electrical input to model the sub-surface resistivities in 2D or 3D, has been highlighted in several works [12–18]. However, although ERT has also been applied in coastal studies (e.g., [19]), there seems to be a limited number of examples of combined applications of HVSR and ERT in sandy beach environments.

In the last decade, SfM- UAV photogrammetry has emerged as an essential technique in medium-scale geological and geomorphological investigations [20–22] due to the possibility of obtaining high-resolution 3D models, orthomosaics and digital elevation models, complemented by its versatility, cost-effectiveness and rapid data acquisition times.

We selected two pocket beaches in Malta as case studies. Pocket beaches are a common and important feature in the Maltese archipelago, with great ecological and economic significance to the country. A pocket beach is a beach, usually of small dimensions, which is isolated between two headlands [23]. Generally, these are semi-restricted systems, as there is little connection between pocket beaches and headlands tend to regulate and store sediment transport within the beach [24]. However, even if their headlands provide them with some protection, they may be extremely sensitive to low-frequency, high-energy storm events [25] that repeatedly hit the Maltese coasts.

While some works have been carried out concerning coastal studies on the Maltese sandy beaches [26–32], there is a lack of studies that consider a three-dimensional perspective including volumetric computation. In a context where the coastal zone will be among the environments worst affected by projected climate change [33], a precise characterization of those environments is essential to better manage these extremely fragile natural resources.

2. Area of Study

2.1. The Maltese Archipelago

The Maltese archipelago is located in the central Mediterranean area, approximately 100 km south of Sicily. It consists of three main islands: Malta, Comino and Gozo (Figure 1). These islands represent the emerged portion of a wide shallow-water platform. The geology of Malta [34–36] is characterized by a sedimentary sequence comprising four major geological formations (Figure 1). Starting from the oldest formation (Fm), the Lower Coralline Limestone Fm (LCL) is a hard and compact pale grey limestone of the Oligocene age. Globigerina Limestone Fm (GL) is a fine-grained yellowish limestone of the Aquitanian–Langhian age (Lower Miocene). The Blue Clay Fm (BC), consisting of bluish or greyish pelagic clay and limestone, belongs to the Serravallian age (Middle Miocene). Lastly, the Upper Coralline Limestone Fm (UCL) is a coarse-grained pale grey

and orange limestone, of the Tortonian–Messinian age (Upper Miocene). Generally, the southeastern part of the island of Malta is shaped by outcrops of LCL and GL, resulting in relatively flat to gently undulating landscapes. The northwestern part of Malta, as well as Comino and Gozo, generally display the complete stratigraphic sequence, where a NE–SW trending horst and graben structure controls flat-topped hills and valleys. Additionally, the islands and the geological sequence have a gentle overall tilt towards the northeast (<10°). These characteristics are the main controlling factors of coastal morphologies: high and sub-vertical cliffs dominate the west coast, while the east side features a smoother coastline. Pocket beaches and embayed areas interrupt the rocky coastline and are typically associated with the NE–SW trending valleys, especially in the northern part of the island of Malta.

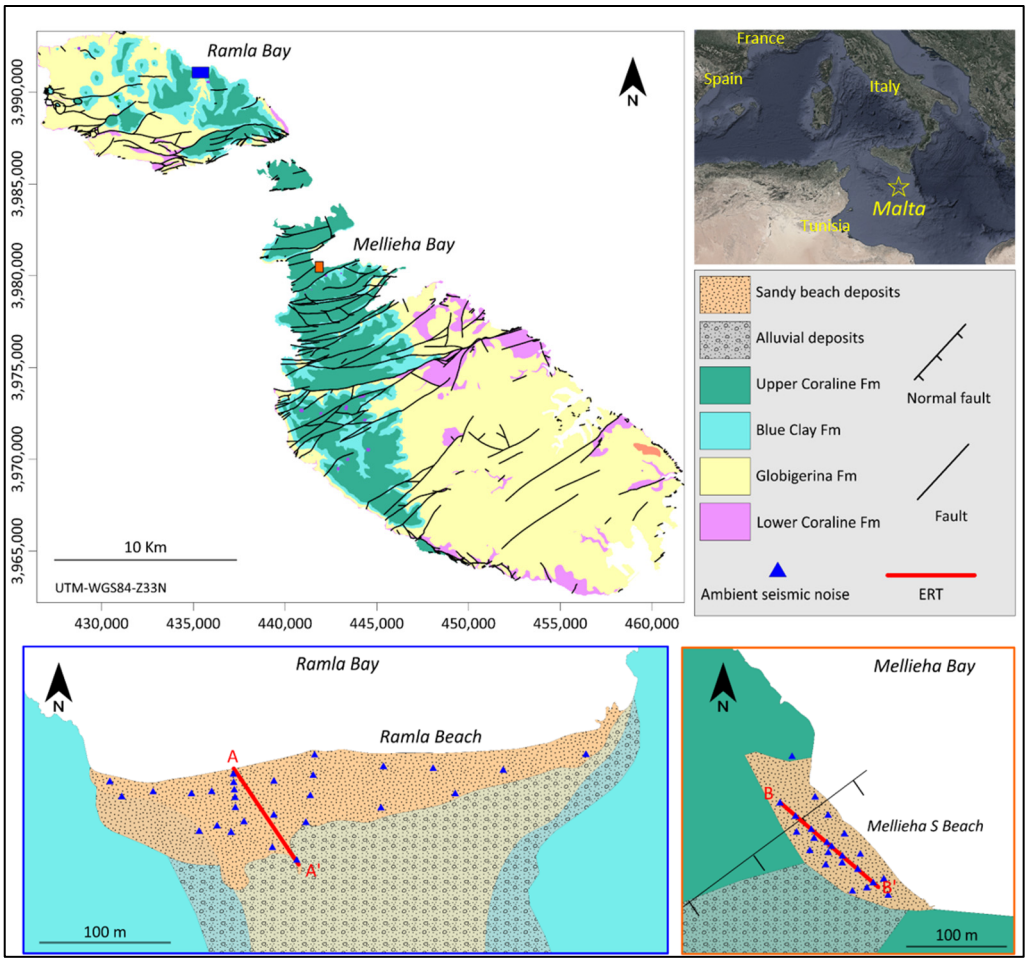

Figure 1. Geological map of the Maltese archipelago. The top right inset shows its position in the Mediterranean Sea. The study areas (Ramla Beach and Mellieha S Beach) are shown in the bottom images with the geophysical measurements presented in this work.

Regarding the recent sedimentary deposits, they are scarce and very localized. Some valleys contain a thin layer of alluvial deposits, typically exhibiting reddish colorations due to iron oxides formed during long-lasting periods of subaerial weathering. The beach deposits represent less than 2.5% of the Maltese coast [37]. These beaches are deposits of gravel and sand, which are predominantly composed of carbonates and subordinately by silts, and originate mainly from the erosion of coastal and shelf Cenozoic limestones and clays and deposited during the Holocene [26,27,30].

2.2. Case Studies

We present two case studies on two iconic beaches of Malta, the one located in Ramla Bay and one on the southern side of Mellieha Bay (Figure 1).

Ramla Bay is located in the northeast of the island of Gozo, at the mouth of a river valley that currently hosts intermittent streams that are functional during storms and runs approximately from south to north. The distance between the headlands that border the bay is approximately 1000 m while the length of the Ramla Beach coastline is nearly 400 m. It is the best-known beach in Gozo, known for its golden-reddish sand, which gives it its name in Maltese (Ramla il-Ħamra) and distinguishes it as unique in the Maltese Islands. The beauty and fragility of this bay fully justify its detailed study.

The slopes that delimit the bay are composed of the BC Fm, and at their highest point, they are crowned by the UCL Fm. Behind the beach deposits, the bay features vegetated dunes and the development of a wetland area, providing it with high ecological importance. The bay holds archaeological and historical interest [38,39] as it houses Roman remains covered by dune sand, a submerged seawall, structures built by the Knights of the Order of St. John in the mid-18th century and the famous Calypso Cave on the western slope.

Mellieha Bay, also known as Għadira bay, is the largest bay in the archipelago, with a width of 1.75 km between the headlands. It contains beach deposits stretching for approximately 850 m. It is a popular beach that is easily accessible from a coastal road that runs along its inland boundary.

This bay represents the northeastern outlet of the Mellieha Valley, which is carved mainly on UCL Fm rocks and has a thin layer of recent sedimentary deposits in its central portion. The valley is bounded on its edges by normal faults forming a graben-like structure. In the centre of the valley, there is a topographic high that crosses it longitudinally, dividing it into two parts. This small hill has higher altitudes at its western boundary; however, it acts as a divide along the entire length of the valley, leading into two small beaches at Mellieha Bay: the northern beach, approximately 500 m long, and the southern beach, about 140 m long, which is the focus of our study and what we call Mellieha S Beach.

3. Materials and Methods

The methodological process employed in this study covers both the surface and subsurface domains of the study sites (Figure 2). To examine the surface of the case studies, field observations were complemented by the generation of 3D photogrammetric models. These models provided orthomosaics and DTMs, allowing for a detailed characterization of the surface. In the subsurface analysis, two near-surface geophysical techniques were employed. Using ambient seismic noise and the HVSR technique, sediment thickness was estimated at different locations along the beaches. These results were interpolated to obtain a continuous interface estimate. Independently obtained ERTs were employed to construct geological sections, providing essential support for determining the average shear wave velocity (Vs) used in thickness estimates derived from the HVSR data. The combination of the surface and subsurface results was ultimately used to assess the sedimentary deposits distribution on the beaches.

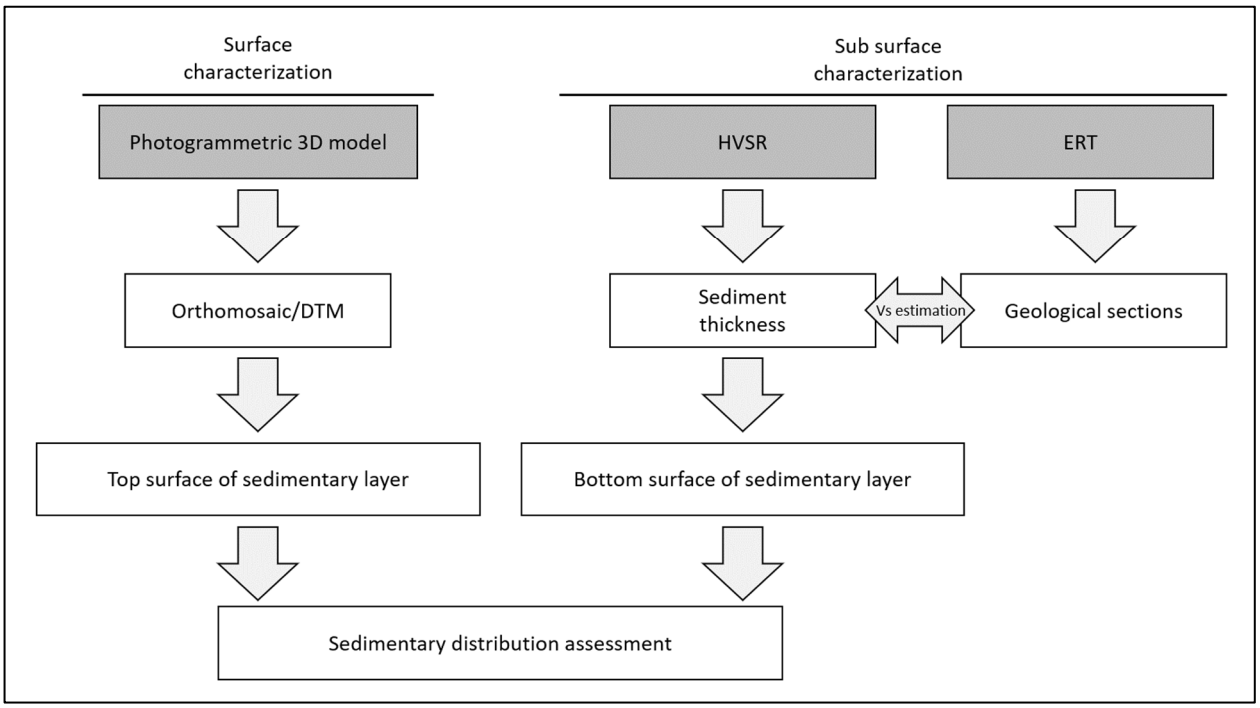

Figure 2. Methodological approach flowchart.

3.1. SfM Photogrammetric Survey

Ramla Bay and Mellieha Bay were surveyed using a Phantom 4 Pro UAV in October 2019, employing a pre-programmed flight function that ensured a constant flight altitude and correct overlap between consecutive images (details in Table 1). The acquired images were processed using Agisoft Metashape v. 2.0.0, a digital photogrammetry software that integrates computer vision algorithms such as SfM. This system allows for the estimation of the 3D position of points represented in multiple images, reconstructing the geometry of the object and the camera position, even if internal orientation parameters are not defined. The photogrammetric processing followed a typical workflow involving a series of consecutive steps [20,40].

Table 1. Details of the photogrammetric data acquisition.

Site	Mellieha Bay	Ramla Bay
Date	October 2019	October 2019
Processed images	573	892
Flight altitude	70 m	75 m
Frontal overlap	80%	80%
Lateral overlap	75%	75%
GCPs	21	35

The first step in the photogrammetric workflow was importing the images into the software, avoiding the defective pictures (e.g., out of focus, overexposed). The subsequent step, known as camera alignment, automatically oriented the images in space. This was followed by the creation of a sparse point cloud, forming a 3D point cloud with scattered points. In the next phase, the software used the camera locations and the sparse point cloud to build a dense point cloud. From this dense point cloud, a continuous surface composed of polygons, with the vertices representing the points in the dense cloud, was reconstructed. This step is referred to as mesh reconstruction, and upon applying texture to this model, a textured 3D model was obtained.

The 3D models were accurately scaled and georeferenced using ground control points (GCPs) that were positioned with high precision using a differential Global Navigation Satellite System (GNSS) before image acquisition. Finally, orthomosaics and digital terrain models (DTMs) were extracted from the 3D model.

3.2. Electrical Resistivity Tomography

Two ERT surveys were conducted on the beach deposits (Figure 1). One was carried out at Ramla Beach (May 2020), perpendicular to the coastline and crossing a dune, using 64 electrodes spaced at 1.5 m, with a total array length of 94.5 m, while the other ERT was performed at Mellieha S Beach (February 2022), parallel to the shoreline, using 64 electrodes and 2 m spacing, reaching 126 m of length. The choice of ERT direction was intended to capture maximum geological variability. In the case of Ramla, the ERT was acquired including shoreline beach deposits and dune deposits. At Mellieha S Beach, the ERT covered both sandy beach deposits and an outcrop of the UCL fm. The instrument used was a multichannel digital resistivity meter ELECTRA (Moho srl) featuring a waveform D/A converter with continuous current and voltage control, including feedback. The applied current during measurements was ±10 mA. The Wenner alpha array was employed for both cases [41]. This multi-electrode array is better suited for recovering vertical resistivity contrasts, and thus it is ideal in geological settings with stratified structure and gently dipping bedding, as in our case (sub-horizontal sands overlying a shallow basement).

To assess the quality of electrode–substrate coupling, impedance measurements were performed for each profile. High impedance values (>3000 Ohm) were found for some electrodes in very-dry sandy areas. To improve the electrode–soil contact, the soil on such electrodes was moistened with a saline water solution. To ensure accurate positioning of the electrodes, GNSS equipment was employed. Topographic information was incorporated into the ERT data to calculate apparent resistivity. To convert the pseudo section of apparent resistivity derived from the field data into a 2D model of real resistivity, we employed the Res2DInv software v. 4.08. We employed a robust inversion that usually best resolves sharp conductivity boundaries [42–44]. The absolute error at Ramla beach after 5 iterations was 21.5%, and the absolute error at Mellieha beach after 4 iterations was 17.3%. Despite these relatively high errors, the models developed demonstrated a robust correspondence with the local geology. In complex geological environments, electrical images tend to experience errors over 15% and, in many cases, reducing these errors without introducing artefacts is not possible [45,46].

3.3. Ambient Seismic Noise Measurements

We acquired 28 ambient seismic noise measurements at Ramla Beach and 23 at Mellieha S Beach (Figure 1). We employed 3 triaxial accelerometer devices Tromino to record ambient seismic noise continuously for 16–20 min at each station, using a sampling rate of 128 Hz. Most of the measurements were performed on sandy beach sediments. To obtain a good device–soil coupling and minimize wind effects, the devices were deployed in holes of 20 cm depth where the sand was mechanically compacted. At each beach, one measurement was taken on rock outcrops. For Ramla Beach, in the GL Fm outcrop located at the western limit of the beach, and for Mellieha S Beach, in the northwestern beach limit, on a UCL Fm outcrop (Figure 1).

The acquired ambient seismic noise signals were processed using the HVSR technique [4]. The processing of the ambient seismic noise data followed a standard workflow [47] in the software Grilla v. 9.7.2. First, we divided the signal into 20 s time windows and selected the most stationary ones by applying an anti-triggering algorithm to avoid transient noise during the analysis. Next, we computed and smoothed the Fourier amplitude spectra for each time window. The two horizontal components were then averaged using a quadratic mean to obtain a representative value. Subsequently, the HVSR function was computed for each window by dividing the amplitude of the horizontal component

average by the vertical component. Finally, the average HVSR function was calculated by averaging the results obtained from all the selected time windows.

The HVSR curves can exhibit peaks at different frequencies. The fundamental premise for interpreting them is to consider that the substrate can be described as a soft sedimentary layer with low shear wave velocity (Vs) lying over a higher Vs bed-rock. The frequency at which the dominant peak occurs is generally related to the sediment thickness and its Vs. Usually, peaks at higher or lower frequencies of the curve correspond to shallower or deeper subsoil features, respectively.

4. Results

4.1. Photogrammetric Analysis

The SFM analysis conducted at Ramla Bay and Mellieha Bay produced accurate results. The DEMs presented resolutions of 5.66 cm/pixel and 5.9 cm/pixel and the orthophotos a resolution of 1.42 cm/pixel and 1.48 cm/pixel, respectively, and point clouds with an RMS reprojection error of 0.92 and 0.56 pixels. More details are summarized in Table 2.

Table 2. Details of the SfM photogrammetric process.

	Ramla Bay	**Mellieha Bay**
Point Cloud		
Points	638,628 of 745,883	221,216 of 311,141
RMS reprojection error	0.178743 (0.928461 pix)	0.214614 (0.567595 pix)
Max reprojection error	3.86717 (47.1645 pix)	2.86192 (28.6239 pix)
Mean key point size	4.11674 pix	2.19475 pix
Point colors	3 bands, uint8	3 bands, uint8
Average tie point multiplicity	4.39553	7.87079
Dense Point Cloud		
Points	81,101,105	39,735,110
Point colors	3 bands, uint8	3 bands, uint8
Model		
Faces	4,937,852	2,389,756
Vertices	2,531,384	1,229,757
Vertex colors	3 bands, uint8	3 bands, uint8
Texture	8096 × 8096, 4 bands, uint8	9096 × 9096, 4 bands, uint8
Source data	Dense cloud	Dense cloud
DEM		
Size	29,338 × 22,523; 5.66 cm/px	23,579 × 27,507; 5.9 cm/px
Source data	Dense cloud	Dense cloud
Orthomosaic		
Size	94,923 × 54,443; 1.42 cm/px	52,139 × 64,799; 1.48 cm/px
Colors	3 bands, uint8	3 bands, uint8

In Ramla Bay, natural geomorphological features were found to be better preserved due to lower anthropogenic influence. The beach at this site is partially enclosed towards the valley and is limited by a system of fixed dunes covered with vegetation. Small marshy areas develop among these dunes, creating a marshland environment, and some agricultural activity is observed in the area. Steep rocky formations limit the sides of the beach. Towards the western boundary, the beach is delimited by the outcrop of the BC Fm, and at its bottom the transitional contact with the GL Fm has a slight sub horizontal

dip to the northeast. GL Fm., with greyish tones in this sector, acts as the bedrock for the beach sediments. As for the eastern boundary of the beach, it is composed of slope deposits and outcrops of the BC Fm. The stratigraphic boundary with the GL Fm is not exposed, presumably due to burial by beach sediments (Figure 3a). The area of sand accumulation was determined to be 14,062 m^2, with 18,344 m^3 of sand above sea level.

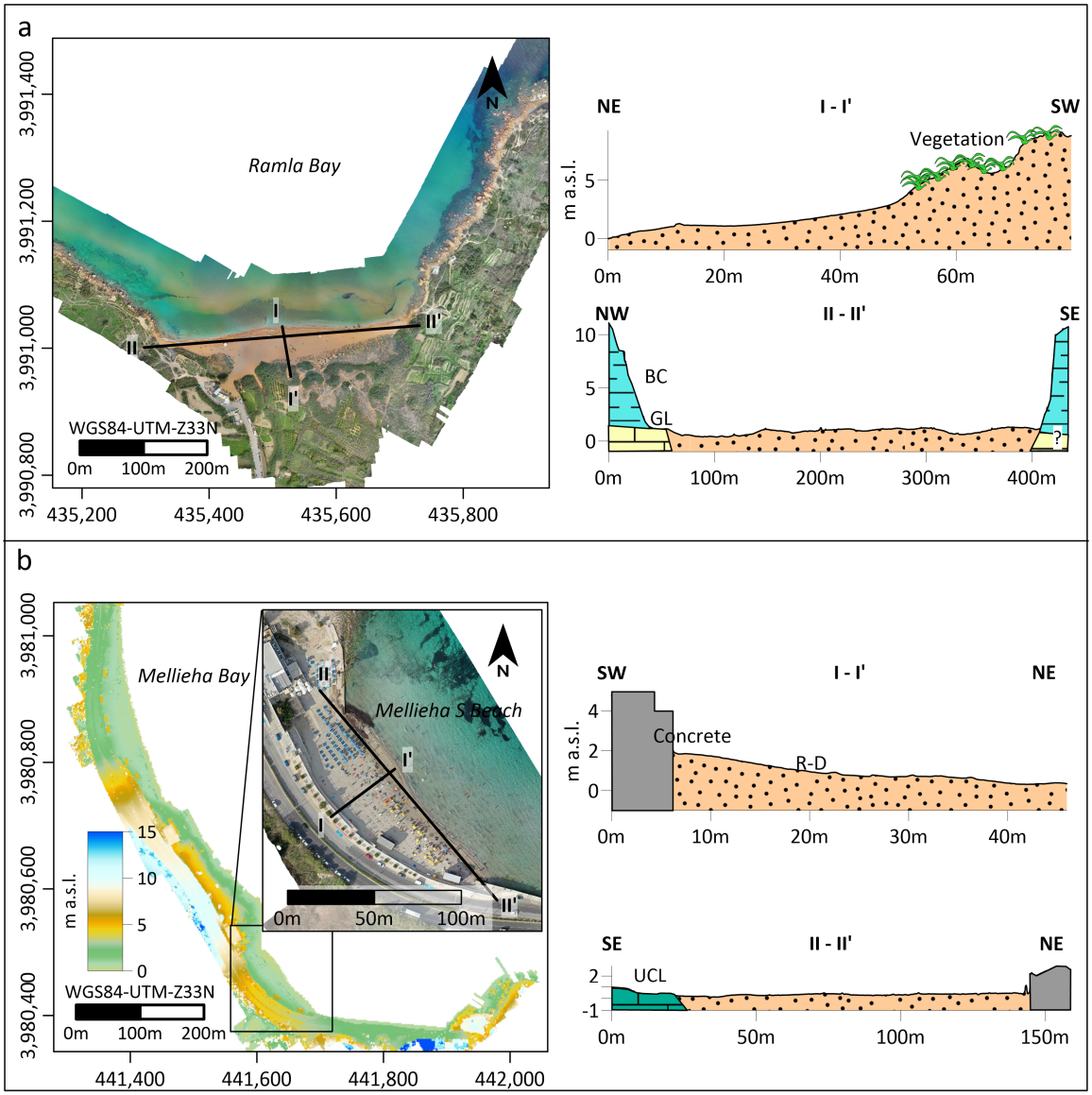

Figure 3. Surface characterization. (**a**) Orthomosaic of Ramla Bay and position of profiles presented on the right: I-I′ orthogonal to the coastline, II-II′ parallel to the coastline. (**b**) DTM of Mellieha Bay and ortho-mosaic of Mellieha S Beach showing the position of the profiles presented: I-I′, orthogonal to the coastline and II-II′, parallel to the coastline. Main surface geological features are labelled and characterized: R-D: recent deposits (mainly sand); UCL: Upper Coralline Limestone Fm; BC: Blue Clay Fm; GL: Globigerina Limestone Fm.

The southern beach of Mellieha Bay, which was the focus of this study, is constrained by a small topographic high to the northwest. This topographic high is composed of UCL Fm and is accompanied by a building that acts as a barrier for sediment in that direction (Figure 3b). Additionally, the beach forms a semi-circular enclosure towards the southwest and southeast and is surrounded by a concrete barrier where a coastal road is located. This configuration traps beach sediments, preventing their movement

towards the mainland. The beach lacks dunes or other significant accumulation or erosion landforms, and typically experiences high levels of recreational use. The area covered by beach deposits was estimated to be 4717 m^2, while the volume of sediments above sea level amounts to 4099 m^3.

Regarding the nature of the deposits, both beaches are predominantly composed of sand-sized sediments. However, Ramla Bay stands out for the notable presence of limestone clasts with decimeter dimensions scattered throughout the beach, within a matrix of sandy sediments. These clasts are likely derived from the UCL, which caps the BC Fm and undergoes significant slope erosion processes, especially in the headlands, as described in previous studies [20,40]. These clasts would be transported to the bay by wave action and littoral currents and then deposited onto the beach during storm events.

4.2. ERT Results

In Ramla Beach, ERT A-A' runs orthogonally to the shoreline (Figure 1). The resistivity model (Figure 4) revealed maximum resistivity values exceeding 3500 Ohm·m in the elevated area corresponding to partially vegetated sandy deposits of a dune. These values were interpreted and supported by field observations, as indicative of unsaturated sand with low moisture content. Beneath this first resistive layer, a continuous layer was observed throughout the entire section, characterized by significantly lower resistivity values of approximately 200 Ohm·m (Figure 4). Within this layer, the minimum resistivity values were found towards the NE limit of the section where the sea is located. This zone of low resistivity was interpreted as saturated beach deposits, where the decrease in resistivity was attributed to an increase in pore water salinity due to the influence of seawater.

At depths close to 4 m b.s.l. and extending to the bottom of the profile, a third domain of resistivities begins on a sub horizontal horizon. This domain exhibits relatively high values that gradually increase with depth, ranging between 500 and 1000 Ohm·m. This domain was interpreted as the limestones of the GL Fm, the rock underlying the sedimentary deposits of the beach. It is worth noting that its surface exhibits a slope towards the sea, likely associated with the marine platform, and a counter-slope inland, probably linked to the archaeological site present in the area [38,39].

The ERT profile B-B' runs approximately parallel to the shoreline of Mellieha S Beach (Figure 1). The model resistivity section exhibits consistently low resistivity values (mostly below 20 Ohm·m) throughout its extent, but a series of resistivity domains separated by high resistivity gradients can be observed (Figure 3).

From x = 30 to the southeastern limit of the section, the shallowest domain showed medium (around 7 Ohm·m) resistivity values. It extends horizontally with a thickness below one meter, from the surface down to elevation 0, and corresponds to the uppermost layer of unsaturated sand. Below this domain, a zone of very-low resistivity values (below 2 Ohm·m) develops, which we interpret as saturated sedimentary deposits containing saline water with high conductivity. This geoelectric domain exhibits a thinning geometry towards the southeast, with maximum thicknesses around x = 40 of about 5.5–7.5 m. Below this domain and towards the bottom of the profile, a third zone with slightly higher resistivity values was interpreted as the UCL Fm. The anomalously low resistivity values for limestone can be associated with a high degree of chemical weathering of the rock, resulting in a greater percentage of clay minerals and an increase in secondary porosity filled with saline water from the sea.

The overall sedimentary body geometry, combined with prior geological information, supports the interpretation of a normal fault zone characterized by a heterogeneous resistivity values zone around x = 20, where the hanging wall block is located in the southeast and hosts the sedimentary deposits.

In general, the results obtained from ERT measurements for beach deposits align with findings from other studies in similar conditions (e.g., [48]), with saline water-saturated sediments typically exhibiting resistivity values below 3 Ohm·m, while dry sand tends to display resistivity values above 1000 Ohm·m. The low resistivity values of the UCL

Fm under conditions of high chemical weathering agree with an ERT survey conducted on a dissected UCL Fm outcrop (Figure 5) at the northwestern boundary of the Mellieha Valley (Figure 1), and contrast with high UCL Fm values obtained in previous studies on the archipelago, although in different conditions [40].

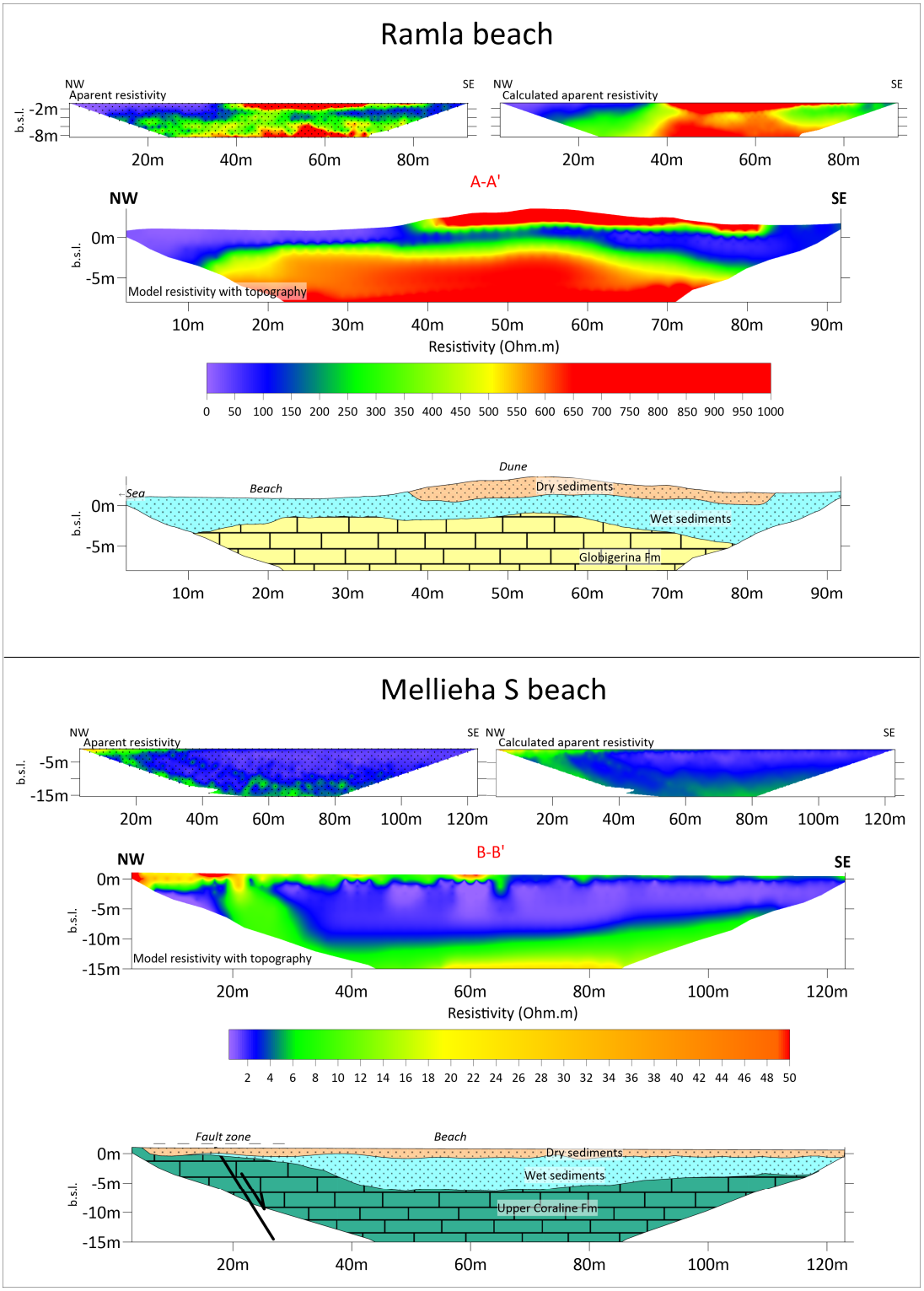

Figure 4. ERT results. For each site, the figure shows the apparent resistivity pseudosection and data distribution, the calculated apparent resistivity pseudosection, the model resistivity with topography and its interpretation. ERTs locations is shown in Figure 1.

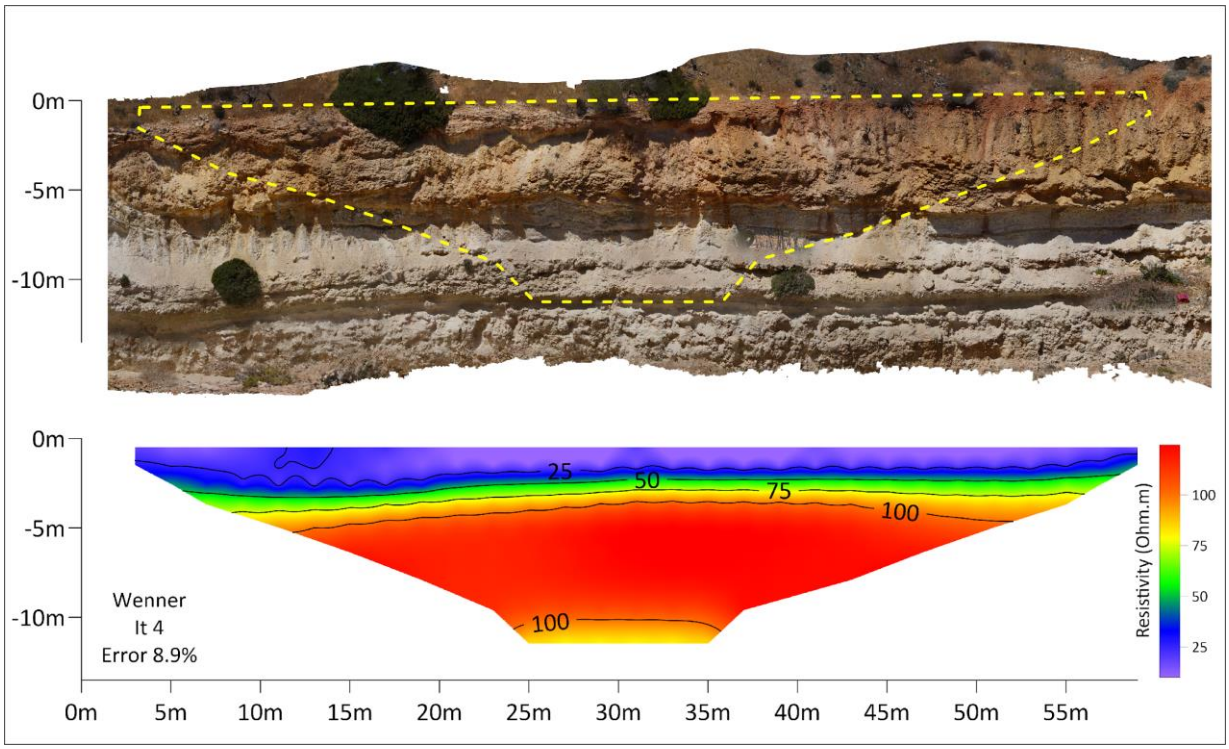

Figure 5. ERT results in a test site in a dissected outcrop in Mellieha Valley, near the Mellieha Bay (Figure 1). The dashed yellow line in the photogrammetric reconstruction shows the ERT results position in the UCL Fm outcrop. Lower resistivity values areas are in the top part of the ERT and coincide with reddish-weathered limestone. Elevations are referred to the ground level.

4.3. HVSR Results

The analysis produced well defined HVSR curves for both sites. To verify the presence of directional effects, the horizontal HVSR were calculated by rotating the NS and EW motion components from 0° (north) to 180° (south) in 10° intervals. Figure 6 displays a typical example of the HVSR and spectral components for each site.

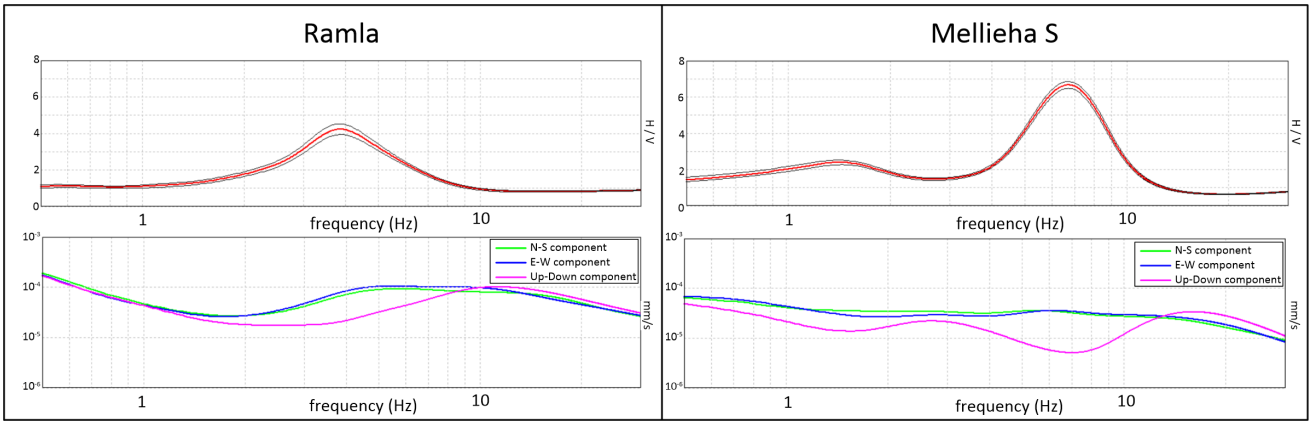

Figure 6. Left: Ramla Beach HVSR example. HVSR peak is present at 3.8 Hz and corresponds with an "eye shape" geometry in the component spectra, where the vertical component presents a fall. Mellieha S Beach HVSR example: Two peaks are present, at 1.5 Hz (F0) and 6.8 Hz (F1). Both peaks correspond with "eye shape" geometry in the component spectra.

The HVSR results from the Ramla Beach exhibit a spectral peak between 2.8 and 7 Hz, with amplitudes ranging from 3 to 7 units, that we call Fs. The results do not show any significant directional amplification effects, as the amplitude of the spectral ratios remained the same for all rotation angles. This and the "eye-shape" of the components spectrum supported a stratigraphic origin of the peaks [47], which we attribute to an impedance contrast resulting from the difference in Vs between the sandy beach deposits with relatively low Vs and the rocky platform of the GL Fm with relatively high Vs. This interpretation is confirmed by the absence of a peak in the HVSR measurement taken at the western boundary of the beach, where sandy sediments were absent, and the measurement was directly performed on the GL Fm.

The HVSR results in Mellieha S Beach exhibit two peaks, one at frequencies between 1 and 2 Hz, that we call F0, and another at frequencies between 6 and 20 Hz, that we call Fs. The measurement taken on the UCL Fm outcrop that bounds the beach on its west side did not exhibit the Fs peak.

The F0 peak, present in all measurements, is interpreted as the result of the impedance contrast between the relatively low Vs BC Fm and the deeper, relatively high Vs GL Fm. This phenomenon has been previously described in various studies conducted on the island (e.g., [49,50]). On the other hand, Fs peaks have been interpreted similarly to those observed in Ramla Bay, although in this case, they are generated by the impedance contrast between the beach sediments and the UCL Fm.

4.4. Sediment Thickness Estimation from HVSR

After identifying the origin of the Fs peaks of the HVSR spectrum generated by the discontinuity between sediments and bedrock, we proceeded to extract the frequency at which each peak occurs at each station. Using these frequencies, it is possible to estimate the depth at which the interface is found at each site.

Two main approaches have been explored in the literature for HVSR peak-to-depth conversion using sediment Vs and peak frequency: a local approach that utilizes borehole data to calculate a local calibration curve (e.g., [7,51]), and a simpler approach, that uses empiric formulas (e.g., [52]). In this study, considering that we do not have borehole data, we decided to approximate the thickness of the sediments by applying the simple formula H = Vs/4*F, where H represents the thickness and F is the HVSR peak frequency corresponding to the interfaces between sediments and the underlying bedrock. Even if it can be an oversimplified strategy [7], this approach is valid for obtaining a rough understanding of the subsurface [53].

Vs is a highly variable parameter in sediments, influenced by factors such as texture, packing density, porosity, composition or degree of water saturation. To determine the average Vs of the sediments at each site, we employed an iterative approach. We calculated sediment thickness using the formula H = Vs/4F at HVSR stations located at the same positions as the ERTs and then we evaluated different possible values of Vs to identify the best fit (Figure 7).

At Mellieha S Beach, an average Vs of 180 m/s shows a good fit with the resistivity calculated sedimentary deposits. At Ramla, despite the limited number of HVSR stations, an average Vs of 120 m/s seems to be a reasonable value to avoid overestimation of sediment thickness. The selection of those Vs values are in agreement with previous works and typical Vs on sediments [6,49].

To obtain a model of the geometry of the contact between the sediments and the bedrock at each beach, HVSR-derived thickness values at each station were interpolated by an ordinary kriging algorithm [54] obtaining a grid of thickness that represents the bottom surface of the sedimentary layer.

To obtain a sedimentary depth grid, we subtracted the bottom surface of the sedimentary layer grid from the SfM-derived DTMs, which represent the top surface of the sedimentary layer.

In addition, we calculate the sediment volumes on each beach. For this purpose, three well-established numerical integration methods were used: the Extended Trapezoidal Rule, Extended Simpson's Rule and Extended Simpson's 3/8 Rule [55]. We obtained consistent results, with differences below 0.1 m^3 between methods.

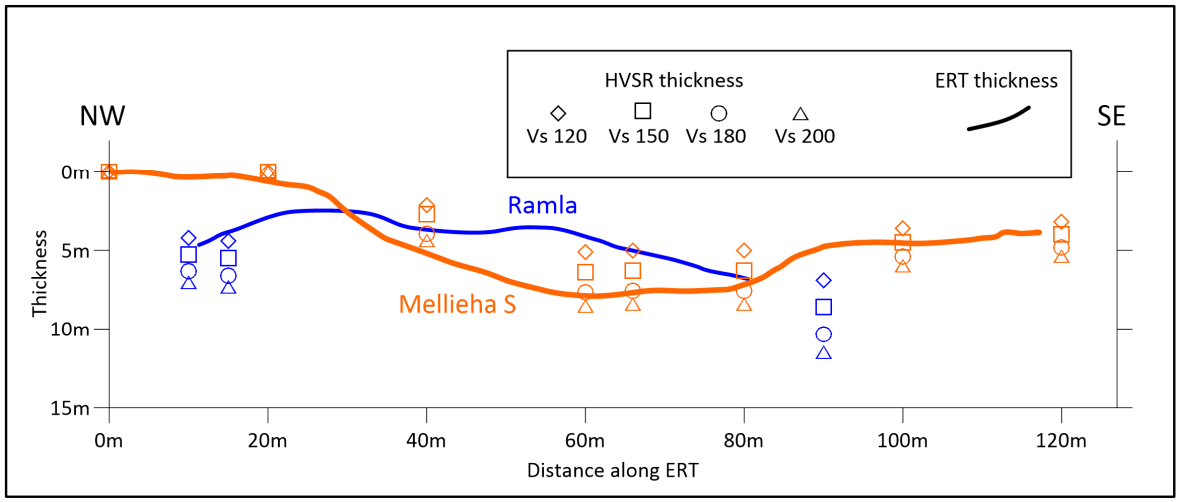

Figure 7. Thickness estimation for Ramla beach (blue) and Mellieha beach (orange) along the ERTs, from the ERTs interpretation and based on the Fs frequencies obtained from HVSR stations utilizing different Vs values.

The results obtained for Ramla Beach (Figure 8) exhibit a total sediment volume of 88,440 m^3 (79% of which is b.s.l.). An ENE trend in the sediment thickness increase is reported, exhibiting a gentle slope (less than 2°) towards the ENE with slight undulations, suggesting that the distribution of the deposits in Ramla Beach is primarily controlled by the stratigraphic contact geometry between the GL Fm, outcropping on the W side of the beach, and the BC Fm, which also exhibits a gentle dip to-wards the ENE (Figure 8b,c). This would have been promoted by the significantly higher erodibility of BC Fm against GL Fm.

In Mellieha S Beach, a total volume of 21,602 m^3 was calculated (72% of which is b.s.l.), which is more than four times lower than Ramla Beach. Maximum thicknesses are observed slightly to the NE of the central sector of the beach, with values close to 7 m (Figure 9a). At the NW boundary, the thickness is minimal and even exposes the UCL, while at the SE boundary of the beach, the thicknesses reach about 3 m. Moving from the center of the beach towards the NW, slope values are about 20°, while the slope towards the SE is less than 5°.

Our interpretation, based both on the ERT and HVSR results, suggests that the geometry of Mellieha S Beach deposits is controlled by structural factors, particularly by the presence of a normal fault (Figure 9b,c). This fault dips to the SW, and the hanging wall block consists of UCL, gently dipping in the opposite direction to the fault.

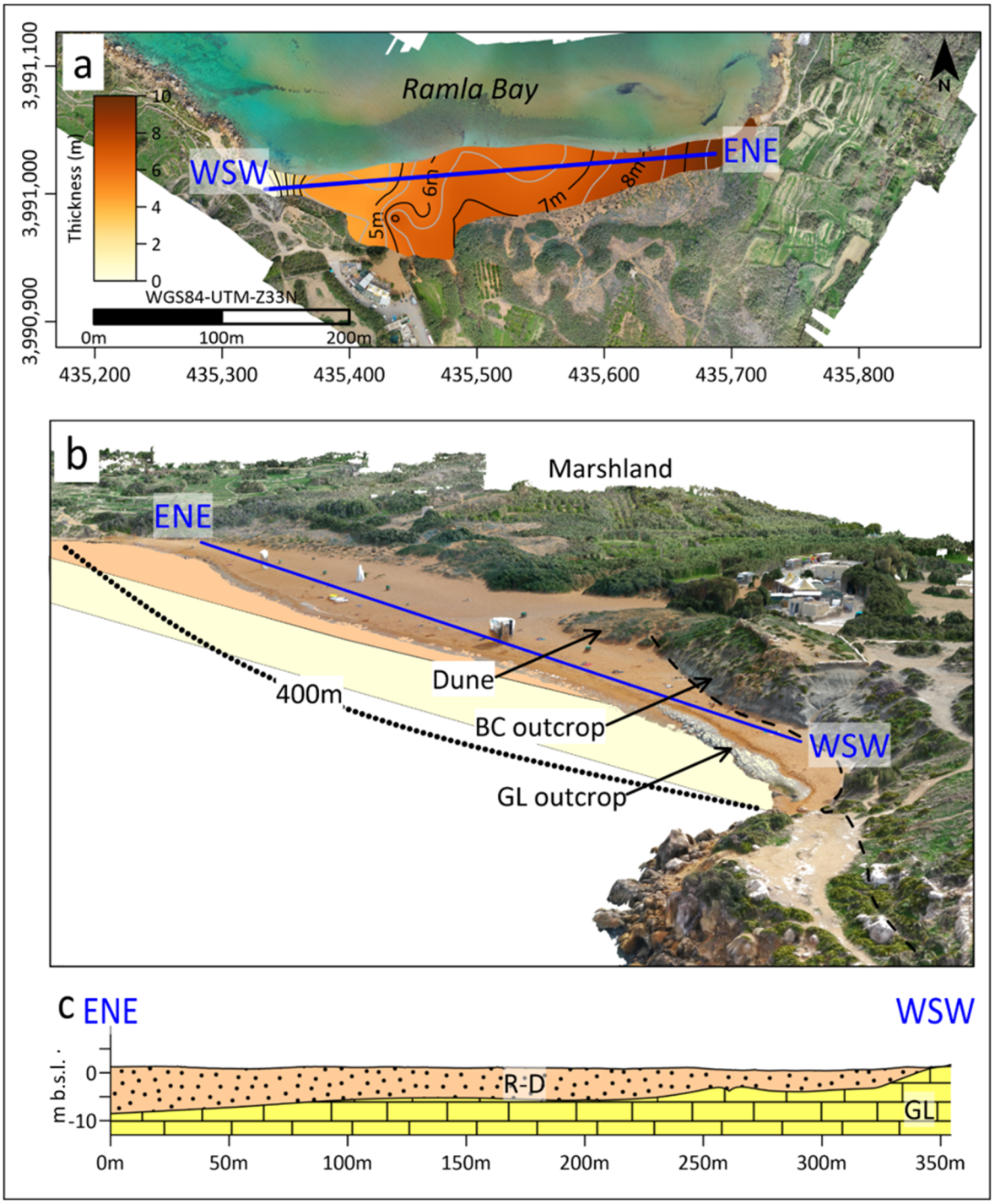

Figure 8. Ramla beach sediment distribution. (**a**) Sediment thickness grid derived from HVSR results. (**b**) 3D photogrammetric model showing main surface features and subsurface representation. (**c**) Cross section of the Ramla Beach, showing the recent deposits resting above the GL Fm.

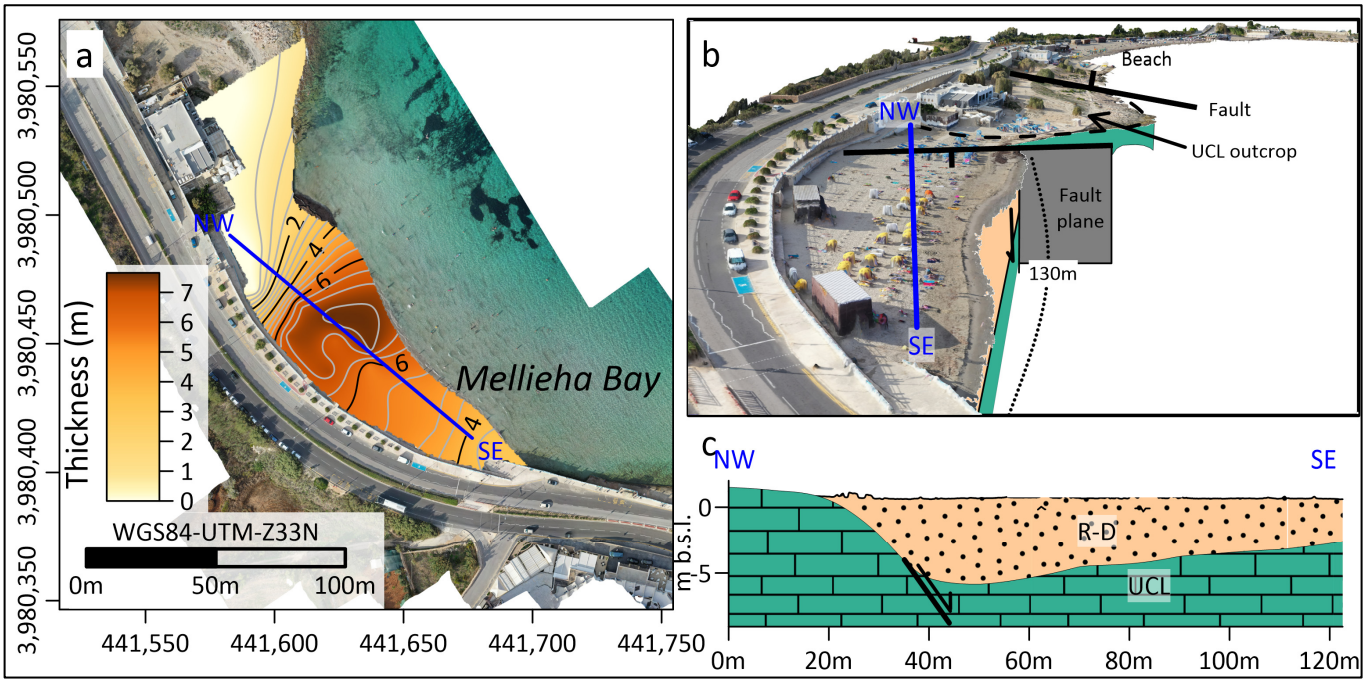

Figure 9. Mellieha S Beach sediment distribution. (**a**) Sediment thickness grid derived from HVSR results. (**b**) 3D photogrammetric model showing main surface features and subsurface representation. (**c**) Cross section of the Mellieha S beach, showing the recent deposits resting above UCL Fm.

5. Discussion

Understanding the sediment distribution in coastal environments is essential for effective coastal management and the preservation of natural resources, especially in a place like Malta where the number of sandy beaches is very low. In this study, we employed a multi-method approach combining ERT, HVSR and SfM photogrammetry techniques to investigate the sediment distribution in two pocket beaches, Ramla Beach and Mellieha S Beach, in Malta.

The results obtained from both ERT and HVSR techniques provided meaningful and consistent findings (Figures 4 and 7–9), enabling the estimation of comparable sediment thickness and morphological characteristics in the studied pocket beaches.

The HVSR maps revealed distinct spatial variations in peak frequencies, which indicated variations in sediment thickness across the study areas (Figures 8 and 9). The observed differences in frequencies were indicative of changes in sediment thickness and provided valuable insights into subsurface properties.

However, it is important to acknowledge the limitations of the study. While efforts were made to obtain comprehensive data coverage, some areas might have been underrepresented, leading to potential gaps in our understanding of sediment distribution in specific regions of the pocket beaches, especially when resolving small-scale features. Furthermore, the geological complexity of the study areas, including the presence of heterogeneities in the bedrock and sediment layers, could have influenced the accuracy of the interpretations. In the absence of borehole data, the direct validation of the geophysical results was not possible. In addition, the selection of the Vs of the sediments, although within the typical ranges, presents a certain degree of uncertainty that is transferred to the HVSR thickness estimation. Despite these limitations, the multi-method approach used in this study provides valuable insights into sediment distribution and subsurface properties of the studied pocket beaches. The findings contribute to our understanding of the main controlling geological factors influencing sediment distribution in the study areas.

6. Conclusions

This study employed a multi-method approach combining HVSR, ERT and SfM photogrammetry from UAV to investigate for first time the volumetric sediment distribution in two pocket beaches in Malta. The results provide valuable insights into the sediment distribution and characteristics of the studied pocket beaches. The HVSR analysis revealed significant variations in sediment thickness, contributing to our understanding of the factors controlling sediment distribution. The ERT data complemented the HVSR results by supporting the modelling of sediment volumes and enhancing the understanding of subsurface resistivities. Additionally, the SfM-UAV photogrammetry technique provided detailed topographic information, enriching our understanding of the beach environments.

This study highlights the importance of considering multi parametric perspectives in coastal studies for accurate characterization of sediment volumes and a better understanding of pocket beach controls. Future research should focus on obtaining borehole data to improve geophysical calibration for sediment thickness estimations.

Given the projected increased vulnerability of coastal zones due to climate change, precise characterizations of coastal environments are even more critical. The multi-method approach used in this study is practical, offering a valuable tool for future coastal studies. The findings can support decision-making processes and the development of sustainable coastal protection strategies to mitigate the impacts of climate change.

Author Contributions: Conceptualization, L.G. and S.D.; methodology, L.G., E.C., P.I., F.V. and S.D.; software, L.G.; validation, L.G. and S.D; formal analysis, L.G., F.V. and S.D.; investigation, L.G., E.C. and P.I., resources, S.D.; data curation, L.G., E.C. and P.I.; writing—L.G. and S.D.; writing—review and editing, L.G., S.D., E.C., P.I., L.R., F.V. and P.G.; visualization, L.G.; supervision, S.D. and F.V.; project administration, S.D., L.G. and E.C.; funding acquisition, L.G., S.D. and F.V. All authors have read and agreed to the published version of the manuscript.

Funding: This work was partially supported by the project Satellite Investigation to study POcket BEach Dynamics (SIPOBED, SRF-2021-2S1, PI: Sebastiano D'Amico),the project Multi-disciplinary monitoring system for a resilient management of coastal areas (REMACO) funded by the INTERREG V A–Italy-Malta Capitalization Programme, the INGV Project "Ricerca 703 Libera" BR2019.23 ("Unveiling silent faults in low strain-rates regions through the integration 704 of high-resolution geophysical and seismological analyses" P.I. Fabio Villani), and by the Internationalisation Partnership & Awards Scheme Plus (IPAS+) supported by the Malta Council for Science and Technology through the project "Near-surface geophysics and geomatic applied to coastal systems" (IPAS-2022-020).

Data Availability Statement: The data presented in this study are available on request from the corresponding author.

Conflicts of Interest: The authors declare no conflict of interest.

References

1. Do, K.; Yoo, J. Morphological Response to Storms in an Embayed Beach Having Limited Sediment Thickness. *Estuar. Coast. Shelf Sci.* **2020**, *234*, 106636. [CrossRef]
2. Cooper, N.J.; Pontee, N.I. Appraisal and Evolution of the Littoral 'Sediment Cell'Concept in Applied Coastal Management: Experiences from England and Wales. *Ocean Coast. Manag.* **2006**, *49*, 498–510. [CrossRef]
3. Morgan, D.; Gunn, D.; Payo, A.; Raines, M. Passive Seismic Surveys for Beach Thickness Evaluation at Different England (UK) Sites. *J. Mar. Sci. Eng.* **2022**, *10*, 667. [CrossRef]
4. Nakamura, Y. A Method for Dynamic Characteristics Estimation of Subsurface Using Microtremor on the Ground Surface. *Railw. Tech. Res. Inst. Q. Rep.* **1989**, *30*, 25–33.
5. Okada, H.; Suto, K. *The Microtremor Survey Method*; Society of Exploration Geophysicists: Houston, TX, USA, 2003; ISBN 978-1-56080-174-0.
6. Villani, F.; D'Amico, S.; Panzera, F.; Vassallo, M.; Bozionelos, G.; Farrugia, D.; Galea, P. Shallow high-resolution geophysical investigation along the western segment of the Victoria Lines Fault (island of Malta). *Tectonophysics* **2018**, *724–725*, 220–233. [CrossRef]
7. Johnson, C.; Lane, J. Statistical Comparison of Methods for Estimating Sediment Thickness from Horizontal-to-Vertical Spectral Ratio (Hvsr) Seismic Methods: An Example from Tylerville, Connecticut, Usa. In Proceedings of the Symposium on the Application of Geophysics to Engineering and Environmental Problems, Denver, CO, USA, 20–24 March 2016; pp. 317–323.

8. Liang, D.; Gan, F.; Zhang, W.; Jia, L. The Application of HVSR Method in Detecting Sediment Thickness in Karst Collapse Area of Pearl River Delta, China. *Environ. Earth Sci.* **2018**, *77*, 259. [CrossRef]
9. Alonso-Pandavenes, O.; Torres, G.; Torrijo, F.J.; Garzón-Roca, J. Basement Tectonic Structure and Sediment Thickness of a Valley Defined Using HVSR Geophysical Investigation, Azuela Valley, Ecuador. *Bull. Eng. Geol. Environ.* **2022**, *81*, 210. [CrossRef]
10. Mohamed, A.M.E.; El-Hussain, I.; Deif, A.; Al-Jabri, K.; Al-Habsi, Z.; El-Hady, S. Near-Surface Site Characterization at Quriyat City, Sultanate of Oman Using HVSR and MASW Techniques. *Arab. J. Geosci.* **2015**, *9*, 23. [CrossRef]
11. Nelson, S.; McBride, J. Application of HVSR to Estimating Thickness of Laterite Weathering Profiles in Basalt. *Earth Surf. Process. Landf.* **2019**, *44*, 1365–1376. [CrossRef]
12. Nguyen, F.; Jongmans, D.; Pirard, E. Near-Surface Geophysical Imaging and Detection of Slow Active Faults. Ph.D. Thesis, Faculty of Applied Sciences, Liège University, Liège, Belgium, 2005.
13. Soupios, P.; Papadopoulos, N.; Papadopoulos, I.; Kouli, M.; Vallianatos, F.; Sarris, A.; Manios, T. Application of Integrated Methods in Mapping Waste Disposal Areas. *Environ. Geol.* **2007**, *53*, 661–675. [CrossRef]
14. Danneels, G.; Bourdeau, C.; Torgoev, I.; Havenith, H.-B. Geophysical Investigation and Dynamic Modelling of Unstable Slopes: Case-Study of Kainama (Kyrgyzstan). *Geophys. J. Int.* **2008**, *175*, 17–34. [CrossRef]
15. Benjumea, B.; Macau, A.; Gabàs, A.; Bellmunt, F.; Figueras, S.; Cirés, J. Integrated Geophysical Profiles and H/V Microtremor Measurements for Subsoil Characterization†. *Near Surf. Geophys.* **2011**, *9*, 413–425. [CrossRef]
16. Gallipoli, M.R.; Giocoli, A.; Piscitelli, S. Joint Application of Low-Cost, Fast Executable and Non-Invasive Geophysical Techniques during Emergency and Microzonation Study: Hints from L'Aquila (Italy) Earthquake. In Proceedings of the Geotechnical and Geophysical Site Characterization: Proceedings of the 4th International Conference on Site Characterization ISC-4, Porto de Galinhas, Brazil, 18–21 September 2012; Volume 1, pp. 1477–1484.
17. Sauret, E.S.G.; Beaujean, J.; Nguyen, F.; Wildemeersch, S.; Brouyere, S. Characterization of Superficial Deposits Using Electrical Resistivity Tomography (ERT) and Horizontal-to-Vertical Spectral Ratio (HVSR) Geophysical Methods: A Case Study. *J. Appl. Geophys.* **2015**, *121*, 140–148. [CrossRef]
18. Abu Zeid, N.; Corradini, E.; Bignardi, S.; Nizzo, V.; Santarato, G. The Passive Seismic Technique 'HVSR' as a Reconnaissance Tool for Mapping Paleo-Soils: The Case of the Pilastri Archaeological Site, Northern Italy. *Archaeol. Prospect.* **2017**, *24*, 245–258. [CrossRef]
19. Zarroca, M.; Bach, J.; Linares, R.; Pellicer, X.M. Electrical Methods (VES and ERT) for Identifying, Mapping and Monitoring Different Saline Domains in a Coastal Plain Region (Alt Empordà, Northern Spain). *J. Hydrol.* **2011**, *409*, 407–422. [CrossRef]
20. Colica, E.; D'Amico, S.; Iannucci, R.; Martino, S.; Gauci, A.; Galone, L.; Galea, P.; Paciello, A. Using Unmanned Aerial Vehicle Photogrammetry for Digital Geological Surveys: Case Study of Selmun Promontory, Northern of Malta. *Environ. Earth Sci.* **2021**, *80*, 551. [CrossRef]
21. Furlani, S.; Antonioli, F.; Colica, E.; D'Amico, S.; Devoto, S.; Grego, P.; Gambin, T. Sea Caves and Other Landforms of the Coastal Scenery on Gozo Island (Malta): Inventory and New Data on Their Formation. *Geosciences* **2023**, *13*, 164. [CrossRef]
22. Leucci, G.; Persico, R.; De Giorgi, L.; Lazzari, M.; Colica, E.; Martino, S.; Iannucci, R.; Galone, L.; D'Amico, S. Stability Assessment and Geomorphological Evolution of Sea Natural Arches by Geophysical Measurement: The Case Study of Wied Il-Mielah Window (Gozo, Malta). *Sustainability* **2021**, *13*, 12538. [CrossRef]
23. Bowman, D.; Guillén, J.; López, L.; Pellegrino, V. Planview Geometry and Morphological Characteristics of Pocket Beaches on the Catalan Coast (Spain). *Geomorphology* **2009**, *108*, 191–199. [CrossRef]
24. Dehouck, A.; Dupuis, H.; Sénéchal, N. Pocket Beach Hydrodynamics: The Example of Four Macrotidal Beaches, Brittany, France. *Mar. Geol.* **2009**, *266*, 1–17. [CrossRef]
25. Pranzini, E.; Rosas, V.; Jackson, N.L.; Nordstrom, K.F. Beach Changes from Sediment Delivered by Streams to Pocket Beaches during a Major Flood. *Geomorphology* **2013**, *199*, 36–47. [CrossRef]
26. Turi, A.; Picollo, M.; Valleri, G. Mineralogy and Origin of the Carbonate Beach Sediments of Malta and Gozo, Maltese Islands. *Boll. Soc. Ceol. Ital.* **1990**, *J09*, 367–374.
27. Gatt, P. Controls on Plio-Quaternary Foreland Sedimentation in the Region of the Maltese Islands. *Boll. Soc. Geol. Ital.* **2007**, *126*, 119–129.
28. Deidun, A.; Gauci, R.; Schembri, J.A.; Šegina, E.; Gauci, A.; Gianni, F.; Gutierrez, J.A.; Sciberras, A.; Sciberras, J. Comparative Median Grain Size Assessment through Three Different Techniques for Sandy Beach Deposits on the Maltese Islands (Central Mediterranean). *J. Coast. Res.* **2013**, *165*, 1757–1761. [CrossRef]
29. Sammut, S.; Gauci, R.; Drago, A.; Gauci, A.; Azzopardi, J. Pocket Beach Sediment: A Field Investigation of the Geodynamic Processes of Coarse-Clastic Beaches on the Maltese Islands (Central Mediterranean). *Mar. Geol.* **2017**, *387*, 58–73. [CrossRef]
30. Gatt, P. Embayment Morphometrics, Granulometry and Carbonate Mineralogy of Sandy Beaches in the Maltese Islands. *Mar. Geol.* **2021**, *432*, 106394. [CrossRef]
31. Randazzo, G.; Italiano, F.; Micallef, A.; Tomasello, A.; Cassetti, F.P.; Zammit, A.; D'Amico, S.; Saliba, O.; Cascio, M.; Cavallaro, F.; et al. WebGIS Implementation for Dynamic Mapping and Visualization of Coastal Geospatial Data: A Case Study of BESS Project. *Appl. Sci.* **2021**, *11*, 8233. [CrossRef]
32. Farrugia, M.T. Public Perceptions on Coastal Erosion in the Maltese Islands: A Case Study of St George's Bay (St Julians) and Pretty Bay (Birżebbuġa). *Nat. Hazards* **2017**, *86*, 587–604. [CrossRef]

33. Cooke, B.C.; Jones, A.R.; Goodwin, I.D.; Bishop, M.J. Nourishment Practices on Australian Sandy Beaches: A Review. *J. Environ. Manag.* **2012**, *113*, 319–327. [CrossRef]
34. Pedley, H.M.; House, M.R.; Waugh, B. The Geology of Malta and Gozo. *Proc. Geol. Assoc.* **1976**, *87*, 325–341. [CrossRef]
35. Pedley, H.M. *The Ghar Lapsi Limestones: Sedimentology of a Miocene Intra-Shelf Graben*; University of Malta Press: Msida, Malta, 1987.
36. Pedley, M. The Calabrian Stage, Pleistocene Highstand in Malta: A New Marker for Unravelling the Late Neogene and Quaternary History of the Islands. *J. Geol. Soc.* **2011**, *168*, 913–926. [CrossRef]
37. Gauci, M.J.; Deidun, A.; Schembri, P.J. Faunistic Diversity of Maltese Pocket Sandy and Shingle Beaches: Are These of Conservation Value? *Oceanologia* **2005**, *47*, 219–241.
38. Ashby, T. Roman Malta. *J. Rom. Stud.* **1915**, *5*, 23–80. [CrossRef]
39. Mifsud, C. Revisiting Ramla L-Ħamra Villa—New Discoveries and Observations on the Roman Villa Complex in Xagħra, Gozo. *Open Archaeol.* **2021**, *7*, 84–97. [CrossRef]
40. Colica, E.; Galone, L.; D'Amico, S.; Gauci, A.; Iannucci, R.; Martino, S.; Pistillo, D.; Iregbeyen, P.; Valentino, G. Evaluating Characteristics of an Active Coastal Spreading Area Combining Geophysical Data with Satellite, Aerial, and Unmanned Aerial Vehicles Images. *Remote Sens.* **2023**, *15*, 1465. [CrossRef]
41. Everett, M.E. *Near-Surface Applied Geophysics*; Cambridge University Press: Cambridge, UK, 2013; ISBN 978-1-107-01877-8.
42. Loke, M.H. Electrical Imaging Surveys for Environmental and Engineering Studies. 1999. Available online: https://pages.mtu.edu/~ctyoung/LOKENOTE.PDF (accessed on 29 October 2023).
43. Loke, M.H.; Dahlin, T. A Comparison of the Gauss–Newton and Quasi-Newton Methods in Resistivity Imaging Inversion. *J. Appl. Geophys.* **2002**, *49*, 149–162. [CrossRef]
44. Loke, M.H.; Acworth, I.; Dahlin, T. A Comparison of Smooth and Blocky Inversion Methods in 2D Electrical Imaging Surveys. *Explor. Geophys.* **2003**, *34*, 182–187. [CrossRef]
45. Naudet, V.; Lazzari, M.; Perrone, A.; Loperte, A.; Piscitelli, S.; Lapenna, V. Integrated Geophysical and Geomorphological Approach to Investigate the Snowmelt-Triggered Landslide of Bosco Piccolo Village (Basilicata, Southern Italy). *Eng. Geol.* **2008**, *98*, 156–167. [CrossRef]
46. Mas-Pla, J.; Rodríguez-Florit, A.; Zamorano, M.; Roqué, C.; Menció, A.; Brusi, D. Anticipating the Effects of Groundwater Withdrawal on Seawater Intrusion and Soil Settlement in Urban Coastal Areas. *Hydrol. Process.* **2013**, *27*, 2352–2366. [CrossRef]
47. Bard, P.-Y. Guidelines for the Implementation of the H/V Spectral Ratio Technique on Ambient Vibrations-Measurements, Processing and Interpretations. Available online: https://scholar.google.com/scholar?cluster=14085203609344808715&hl=en&oi=scholarr (accessed on 29 October 2023).
48. Buquet, D.; Sirieix, C.; Anschutz, P.; Malaurent, P.; Charbonnier, C.; Naessens, F.; Bujan, S.; Lecroart, P. Shape of the Shallow Aquifer at the Fresh Water–Sea Water Interface on a High-Energy Sandy Beach. *Estuar. Coast. Shelf Sci.* **2016**, *179*, 79–89. [CrossRef]
49. Pischiutta, M.; Villani, F.; D'Amico, S.; Vassallo, M.; Cara, F.; Di Naccio, D.; Farrugia, D.; Di Giulio, G.; Amoroso, S.; Cantore, L.; et al. Results from Shallow Geophysical Investigations in the Northwestern Sector of the Island of Malta. *Phys. Chem. Earth Parts A/B/C* **2017**, *98*, 41–48. [CrossRef]
50. Iannucci, R.; Martino, S.; Paciello, A.; D'Amico, S.; Galea, P. Investigation of Cliff Instability at Għajn Ħadid Tower (Selmun Promontory, Malta) by Integrated Passive Seismic Techniques. *J. Seism.* **2020**, *24*, 897–916. [CrossRef]
51. Ibs-von Seht, M.; Wohlenberg, J. Microtremor Measurements Used to Map Thickness of Soft Sediments. *Bull. Seismol. Soc. Am.* **1999**, *89*, 250–259. [CrossRef]
52. Farrugia, D.; Paolucci, E.; D'Amico, S.; Galea, P. Inversion of Surface Wave Data for Subsurface Shear Wave Velocity Profiles Characterized by a Thick Buried Low-Velocity Layer. *Geophys. J. Int.* **2016**, *206*, 1221–1231. [CrossRef]
53. Bignardi, S. The Uncertainty of Estimating the Thickness of Soft Sediments with the HVSR Method: A Computational Point of View on Weak Lateral Variations. *J. Appl. Geophys.* **2017**, *145*, 28–38. [CrossRef]
54. Journel, A.G.; Rossi, M.E. When Do We Need a Trend Model in Kriging? *Math. Geol.* **1989**, *21*, 715–739. [CrossRef]
55. Kalambet, Y.; Kozmin, Y.; Samokhin, A. Comparison of Integration Rules in the Case of Very Narrow Chromatographic Peaks. *Chemom. Intell. Lab. Syst.* **2018**, *179*, 22–30. [CrossRef]